



**The author(s) shown below used Federal funding provided by the U.S. Department of Justice to prepare the following resource:**

**Document Title:** The Fluid Dynamics of Droplet Impact on Inclined Surfaces with Application to Forensic Blood Spatter Analysis

**Author(s):** G. Paul Neitzel, Marc Smith

**Document Number:** 251439

**Date Received:** December 2017

**Award Number:** 2013-DN-BX-K003

**This resource has not been published by the U.S. Department of Justice. This resource is being made publically available through the Office of Justice Programs' National Criminal Justice Reference Service.**

**Opinions or points of view expressed are those of the author(s) and do not necessarily reflect the official position or policies of the U.S. Department of Justice.**

## Abstract

Bloodstain pattern analysis is a technique used in crime-scene reconstruction to determine the point of origin of a blood droplet as well as the method of its creation, e.g., dripping, wiping, or low-to-high-speed impact caused by anything from blunt trauma to cast-off to gunshot wounds. The primary problem of interest in this analysis is to determine of the initial size, speed, and impact angle of a blood droplet that has struck a solid surface through an examination of the bloodstain pattern left on the surface. This research project addressed this problem using a detailed fluid dynamical study of the impact and spreading of a liquid droplet on planar surfaces of variable roughness, wettability, and absorbency oriented at various angles with respect to the velocity vector of the approaching droplet. In particular, this research used a coordinated program of laboratory experiments and numerical simulations to examine the influence of the many parameters associated with such droplet impacts. Given its importance to crime-scene reconstruction, the focus of this work is on how to use the *shape of the final stain* to determine the initial conditions of droplet impact.

The main goals of this research program are as follows: a) quantify the effects of the droplet impact angle, the initial droplet size and speed, and the solid surface roughness and wettability on the pattern of the final observed stain, and b) analyze this data to provide simplified, but relevant phenomenological models of droplet impact, spreading, and splashing that can be directly used by practitioners in the field of forensic science.

The experimental portion of this research used a specially designed droplet generator to create individual liquid droplets of a specified diameter and velocity. The liquid was a specially prepared mixture of water, glycerin, and alcohol that has the same density, viscosity, and surface tension as human blood. These liquid droplets were propelled against three different solid surfaces, i.e., glass, bathroom tile, and paper, held at a specified angle with respect to the vertical. The droplet impact speed was measured by a pair of photodiodes and the impact of the droplet against the surface was recorded with a high-speed video camera held normal to the impact surface. The video images were analyzed to obtain the maximum spreading width and length of the droplet as well as the number of irregularities or projections in the shape of the droplet (spines) that may be present. These data were then analyzed to determine any specific relationships with the main fluid dynamical parameters that govern this impact process, i.e., the Reynolds and Weber numbers.

The development of a numerical simulation of the droplet impact problem was partially completed during this project. When completed, this will be a time-dependent, 3-D, multiphase flow simulation based on a wavelet adaptive grid that was designed from scratch using modern computing techniques optimized for fast parallel processing on a single graphic processing unit (GPU). This simulation will be capable of accurately predicting the motion of a liquid droplet as it impacts and spreads along a solid surface, a typical droplet impact event.

# Table of Contents

|   |    |
|---|----|
| Abstract .....                                | 1  |
| Executive Summary.....                        | 3  |
| I. Introduction .....                         | 10 |
| II. Project Design and Methods.....           | 14 |
| 1) Experimental methods .....                 | 14 |
| 2) Blood simulant .....                       | 16 |
| 3) Numerical methods.....                     | 17 |
| 4) Data analysis.....                         | 17 |
| III. Results.....                             | 19 |
| 1) Experimental work .....                    | 19 |
| 2) Numerical work .....                       | 23 |
| IV. Conclusions .....                         | 24 |
| 1) Discussion of findings .....               | 24 |
| 2) Implications for policy and practice ..... | 25 |
| 3) Implications for further research .....    | 26 |
| V. References .....                           | 27 |
| VI. Dissemination of Research Findings .....  | 29 |

## Executive Summary

### *I. Introduction*

Crime scene reconstruction is the process of determining the events involved with a crime using the physical evidence present at the scene along with scientific methodology and deductive reasoning. Various techniques are used as part of this reconstruction process; including DNA evaluation, fingerprint identification, and the focus of this work, blood spatter analysis. In blood spatter analysis, the residual bloodstains left at the scene of a crime are used to determine the point of origin of a particular bloodletting event and the type of trauma that led to the bloodstain (e.g., gunshot, blunt force, sharp object, etc.). The determination of these factors assists crime-scene analysts in their efforts to establish the sequence of events that occurred during the crime.

The size and shape of a typical bloodstain on a solid surface is the result of the physical characteristics of the blood droplet and the solid surface just prior to impact. The relevant droplet characteristics are the impact angle with respect to the surface, impact speed, droplet size, and the blood material properties of viscosity, density, and surface tension. The relevant characteristics of the solid surface are its average roughness, hardness, wettability, and porosity. The size of a bloodstain is quantitatively described as the area of the stain's circular or elliptical shape, whereas shape is quantified by the bloodstain's aspect ratio as well as the number of spines and satellite drops around the outer contour of the bloodstain.

In a forensics analysis of blood spatter, the size and shape of the bloodstain is used to determine the blood droplet impact conditions, i.e., its impact angle, speed, and size. One long standing correlation in common use relates the impact angle  $\alpha$  to the aspect ratio of the droplet  $Ar$  using the equation  $\sin(\alpha) = W / L = Ar$ , where  $W$  and  $L$  are the width and length (along the impact direction) of the bloodstain. A bloodstain on a solid surface occurs when the blood penetrates, chemically reacts, or just adheres and dries onto the solid surface. When a droplet impacts the surface, it spreads out to a maximum extent and then may or may not retract to some degree back toward the center of impact. The working definition in this project is that the bloodstain left by the spreading droplet corresponds closely to the region of maximum spreading. Note that this initial region of droplet spreading is exactly where the process is most affected by the impact properties of the droplet and the properties of the solid surface.

If the blood droplet does not penetrate, chemically react, or adhere to the solid surface, its final static shape after the spreading and retraction process would be a spherical cap with a circular contact line on the solid surface. In this case, the initial impact information is lost except for the initial droplet size, which would correlate to the final diameter of the circular contact line. Part of any forensic analysis of blood spatter would be to recognize if the impact process in question behaved in accordance to this working definition. If not there would be little point in proceeding further because most of the initial conditions of the droplet impact would be obscured.

The important physical parameters of the droplet associated with the spreading stage of droplet impact are the droplet impact velocity  $V$ , diameter  $D$ , and impact angle  $\alpha$ ; and the fluid properties of

density  $\rho$ , viscosity  $\mu$ , and surface tension  $\sigma$ . The properties of the solid surface are its average roughness, hardness, wettability, and porosity. In this first project, the properties of the droplet are of primary concern, while the effects of the solid properties on the spreading process (particularly the surface roughness) were explored to a lesser extent. The impact and fluid properties can be combined using dimensional analysis to produce two main dimensionless parameters, the Reynolds number  $Re$  and the Weber number  $We$ , defined as follows:

$$Re = \frac{\rho V D}{\mu}, \quad We = \frac{\rho V^2 D}{\sigma}.$$

The Reynolds number is the ratio of inertial to viscous forces and the Weber number is the ratio of inertial to surface tension forces. In a crime scene situation where blood spatter may result from dripping, blunt-force trauma, or gunshot wounds, these dimensionless parameters fall into the following ranges:

|                     |                   |          |
|---------------------|-------------------|----------|
| $240 < Re < 6,000,$ | $20 < We < 2,100$ | dripping |
| $10 < Re < 4,800,$  | $1 < We < 3,400$  | trauma   |
| $1 < Re < 12,000,$  | $1 < We < 85,000$ | gunshot  |

Note that the domains for dripping and trauma are almost the same whereas the higher parameter ranges are typically accessed in a gunshot situation.

Although previous work in the literature provides some valuable insight into various aspects of droplet spreading behavior, many questions still remain. Thus, the main goals of the present research program are as follows:

- a) quantify the effects of the droplet impact angle, the initial droplet size and speed, and the solid surface roughness and wettability on the pattern of the final observed stain defined by the point of maximum droplet spreading, and
- b) analyze this data to provide simplified, but relevant phenomenological models of droplet impact, spreading, and splashing that can be directly used by practitioners in the field of forensic science.

## ***II. Project Design and Methods***

The experimental facility designed for this work has four primary components: a droplet generator, a target assembly, a high-speed video camera, and a control computer. The droplet generator produces a single liquid droplet on demand with a specified size and speed directed vertically downward. It is mounted on a movable platform that can be positioned at a variable vertical distance to the target in order to increase the speed of the droplet using gravitational acceleration. The droplet impacts a solid surface held on the target assembly at a specified angle with respect to the vertical. The target assembly contains a pair of lasers and photodiodes used to measure the impact speed of the approaching droplet. The initial droplet diameter, assuming a spherical droplet, is obtained by measuring the mass of the target surface before and after each droplet impact. The droplet generation and the experimental measurements are controlled and recorded using a personal computer with a Labview interface to the experimental equipment. With this facility, single liquid droplets with

diameters from 2–5 mm can be reliably and predictably produced. Droplet impact speeds can be as high as 5 m/s. In a forensics context, these droplets correspond to those created via dripping or some large droplet, low speed, blunt force trauma situations. Droplets resulting from gunshot wounds are typically much smaller and faster. However, the Reynolds and Weber number ranges covered in these experiments include both dripping and blunt force trauma situations.

The primary data of interest in these experiments is the spreading behavior of the droplet as it spreads along the solid target surface. Images of this process are observed and recorded with a high-speed video camera mounted on the target assembly. The camera is held above the target surface and its view angle of the impact plane is always 90° (normal) even when the target surface is inclined.

Blood is both a viscoelastic and shear thinning fluid. However, for shear rates larger than 100 s<sup>-1</sup>, which are typical in the droplet impact problems seen in this experimental facility, it behaves as if it were a Newtonian fluid. Thus, to simplify the experimental procedures a blood simulant was developed based on a mixture of water, glycerin, and alcohol. The resulting mixture matched the kinematic viscosity of blood at 4.15 cSt and the surface tension of blood at 62 mN/m. Due to the temperature-dependent nature of the viscosity of water-glycerin mixtures, ambient conditions were carefully monitored to ensure that test conditions and liquid properties were maintained at constant values. The simulant liquid was prepared and tested before each experimental run to verify that the properties were correct. A Newtonian blood simulant also provides a baseline study from which the non-Newtonian effects of blood can be explored in a later project.

A numerical simulation of this droplet impact problem was designed from scratch using modern computing techniques optimized for parallel processing on a graphic processing unit (GPU). The 3-D time dependent simulation uses the fluid-flow governing equations for mass, momentum, and energy *written in compressible form since this formulation is ideally suited for GPU parallelization*. Air was treated as an ideal gas and an appropriate equation of state for liquid compressibility was used. The equations are integrated in time using *an implicit dual-time stepping scheme that accurately accounts for the stiffness of the liquid to compute the pressure field during the low-speed incompressible motion typical of a droplet impact event*. The spatial discretization of the equations is based on a fourth-order finite difference scheme with a wavelet adaptive multi-resolution grid to automatically resolve and capture all of the length scales of the motion. The interface of the droplet was modeled using the level-set method.

The high-speed performance of these parallel GPU computations is a direct result of using the compressible form of the underlying flow equations. With this form the computations can more effectively access the memory and computational threads of the GPU. In the droplet impact problem, the effect of compressibility is very small in the liquid, but is important in the gas layer underneath the droplet. This is accounted for in these simulations by an implicit dual-time stepping scheme that integrates the acoustic pressure field on an extremely fast time scale to compute the bulk pressure experienced by each fluid as it moves. In fact, the compressible form of the flow equations is a more accurate reflection of the underlying physics of the flow field and the wave propagation of the acoustic pressure is the physical process through which the bulk pressure field is established in an incompressible flow. The net effect of the fast acoustic field is to maintain an incompressible flow in the domain of the

liquid, i.e., no volume change in the liquid, while allowing for compressibility effects in the gas layer underneath the droplet. Thus, *this GPU simulation with dual time stepping will compute an incompressible flow field in the liquid even though the equations are written in compressible form.*

### **III. Results**

The experimental facility was used to perform 182 experiments with five different impact angles and three different target surfaces: 78 on clean glass, 52 on bathroom tile, and 52 on paper. Over all of these experiments, the aspect ratio of the fully spread droplet is almost constant with Reynolds number, except for a small increase as the Reynolds number increases for an impact angle of 30°. The aspect ratio versus the angle of impact for all experiments follows the common practice relation  $\sin(\alpha) = Ar$  for near normal impact angles. However, this relation under-predicts the impact angle for a given bloodstain aspect ratio for impact angles less than about 40°. These data were fitted in a least-squares sense to a new curve based on the common practice relation with the form

$$\alpha = x + \frac{1}{898} \{90^\circ - x\}^2, \quad x = \text{asin}(Ar).$$

While this relation is useful for all surfaces, the data suggest some effect due to surface roughness for the smaller impact angles. A rougher surface produces a stain with a smaller aspect ratio.

The experimental data was analyzed using some of the phenomenological spreading models available in the literature. For normal droplet impact, the maximum spreading diameter is governed by the transfer of the kinetic energy of the droplet to capillary energy (surface energy of the fully spread droplet) with some energy dissipation through a viscous boundary layer on the solid surface. This suggests a relationship between the width of the spreading droplet in the lateral direction (perpendicular to the impact velocity) and the normal component of the impact velocity. In dimensionless form this relationship is

$$\frac{W_{\max}}{D} Re_n^{-1/5} = f(P), \quad P = We_n Re_n^{-2/5},$$

where  $W_{\max}$  is the maximum lateral spreading width of the droplet, and  $Re_n$  and  $We_n$  are the Reynolds and Weber numbers based on the normal impact velocity. This relationship provides a decent fit to the data although there was not a very large range of the data in this parameter space. It is also clear that there is a dependence of the spreading width on the roughness of the surface.

Other parameters computed for the bloodstain were the eccentricity ratio, defined as  $Ec = (L - W) / D$ ; and the spreading factor,  $S_f = LW / D^2$ . The eccentricity ratio results suggest that this scaling may capture some of the appropriate physics. However, there is significant scatter in the data, which may just be the inherent variability in the data from this experiment. The spreading factor data shows a weak influence of the impact angle, and this effect increases as the Reynolds number increases. The data fit for the spreading factor data seems to be slightly better than the data fit for the eccentricity ratio. There also appears to be a slight surface effect with the data for paper being smaller than those for glass.

When the impact velocity of the droplet is large enough, spines and/or satellite droplets appear in the bloodstain. This indicates either the start or the presence of splashing. The number of spines was plotted using the same scaling parameter  $P$  and the results show a clear effect of the surface roughness on the number of spines that appear during spreading. The glass surface is the smoothest and it has the fewest number of spines. The next smoothest surface is tile, but it seems to have more spines than the roughest surface, which is paper. The surface roughness affects the spreading of the droplet and the subsequent instability of the droplet rim. The mechanism of this interaction is not clear and needs to be studied in future work.

Recent work by Eggers *et al.* [Phys. Fluids 22, 062101, 2010] presented a simple model for droplet spreading on a solid surface with a normal impact velocity. The model is based on the bulk acceleration of the droplet rim driven by a stagnation point flow in the thin film of liquid near the droplet center. In this thin film there is also a boundary layer flow that eventually arrests the stagnation point flow. This model was investigated and improved in several ways in the present work. The results seem to be quite successful for normal impact. It seems likely that this model can be extended to the situation of oblique droplet impact, which is a problem of direct relevance to blood spatter.

The GPU-based, wavelet-adaptive, 3-D, multiphase flow simulation was partially completed during this project. Currently, it can solve for single-phase flow fields under compressible and/or incompressible flow conditions. The wavelet grid allows it to provide fully resolved flow fields and the GPU programming provides extremely fast execution speeds. These capabilities were validated in three example simulations. The level-set formulation to allow for the simulation of multiphase flows was not completed and is still under development.

## ***IV. Conclusions***

### *1) Discussion of Findings*

The experimental findings from this work demonstrate that the common practice relation between the droplet impact angle and the bloodstain aspect ratio, i.e.,  $\sin(\alpha) = Ar$ , is in significant error for shallow impact angle less than about 40°. A new correlation to correct this error was found. While this correlation is based on all of the experiments on three different surfaces, the data indicate that the correction is greater for rougher surfaces, i.e., rougher surfaces produce smaller aspect ratios for the final bloodstain. This is a significant result and the effect is worthy of further investigation.

Simple phenomenological or mechanistic ideas of droplet spreading indicate that the maximum droplet spreading normal to the impact vector is governed by the transfer of the kinetic energy of the droplet to capillary energy (surface energy of the fully spread droplet) with some energy dissipation through a viscous boundary layer on the solid surface. When the experimental data for the lateral width of the droplet are scaled using appropriate scaling parameters that reflect this balance they collapse near a representative curve and compare well with other data in the literature. Again, the roughness of the surface does appear to have some influence where a rougher surface decreases the lateral spreading of the droplet.

Three other bloodstain parameters were examined using these same ideas; the eccentricity ratio, the spreading factor, and the number of spines on the periphery of the bloodstain. The results for the eccentricity ratio and the spreading factor seem to collapse into a single region, but there is still

significant variability in the data. The results for the spreading factor indicate that this variability is not due to variations in the impact angle. The results for the number of spines collapse into a single curve for small values of the parameter  $P$ , but there is a significant surface roughness effect as  $P$  increases.

The variability seen in all of the data is a significant source of concern that needs to be understood. One possible cause may be the droplet generator, since any method of droplet generation will cause droplet oscillations. In addition, droplet deformation and oscillation may also occur due to aerodynamic forces on the droplet as it travels toward the surface. If these oscillations are not damped out before the droplet strikes the surface, the deformed shape of the droplet may affect the spreading process. Another possible cause of the data variability may be variable surface roughness. The roughness of the tile and paper surfaces used may not have had the same roughness from sample to sample, and the roughness of each surface may not have been uniform across the surface. Even for the smooth glass surface, it is known that contamination can affect the droplet spreading process. *To verify the source of the data variability, the experiments need to be repeated with more careful control or at least better characterization of the droplet generation process. There should also be better control on the uniformity and magnitude of the roughness of the impact surfaces. It would also be useful to have a larger number of impact surfaces covering a wider range of roughness magnitude.*

A simple phenomenological or mechanistic model for the spreading of a droplet under normal impact on a surface seems to capture the essential physics of the droplet spreading process. The idea is that the droplet rim is accelerated outward by a stagnation point flow produced by the impacting droplet. The results for an improved version of this model compare well with numerical simulations of droplet spreading and seem to do a good job in predicting the maximum spreading diameter of the droplet.

The GPU-based, wavelet-adaptive, 3-D, multiphase flow simulation was partially completed during this work. In its current form, the simulation is only capable of computing single phase flows. The simulation was verified against a number of well characterized benchmark flow problems, including both compressible and incompressible flows. The comparisons were excellent, with the resolution of the simulation self-adapting to the flow conditions to meet a user-specified error tolerance. The development of the level-set model to enable the wavelet multiphase flow simulation and its use on the droplet impact problem will be the subject of a future investigation.

The first goal of the project was to quantify various parameter effects on the observed pattern of maximum droplet spreading (assumed to characterize a bloodstain). The second goal was to provide useful models of these effects for forensic practitioners. The effects of the droplet impact angle, size, and speed on the maximum spreading aspect ratio were measured and useful correlations were obtained from these data to meet these two goals. In addition, correlations for the number of spines in the final spreading pattern were also found. The measured data showed a clear effect of solid surface roughness and/or wettability on the final spreading pattern, but there was not enough data to fully quantify this effect. The usefulness of these results is limited by the observed variability and scatter in the data, especially for the rougher paper surface. Another limitation is that the results are limited to a forensic parameter range typical of either dripping or blunt force trauma situations.

## *2) Implications for policy and practice*

Bloodstain pattern analysis is an important tool in the criminal justice community. The bloodstain problem of interest to this research is the impact of a blood droplet on a solid surface. The final bloodstain on the surface is the result of very complex fluid dynamical processes involved in the spreading and splashing of the droplet. Thus, it is not surprising that the current simple relations used to predict the droplet impact velocity and angle from the appearance of the final bloodstain do not work well in all cases.

The results of this research have produced a new set of simple correlations for use in bloodstain pattern analysis. From the normal measurements of the length and width of a bloodstain, this work has produced a correction to the standard practice relation used to compute the impact angle of the blood droplet; a correction that depends on the roughness of the surface (the correction is larger for rougher surfaces). This work also developed other correlations for the bloodstain based on the lateral spreading, the eccentricity, the spreading factor, and the number of spines versus an appropriate dimensionless parameter relevant to the impact and spreading process. These correlations can be used together to determine the impact speed and diameter of the blood droplet. However, these predictions have significant error because of the variability of the data seen in these experiments. If this variability can be quantified, it is expected that the use of these correlations would allow for a more accurate assessment of the initial conditions related to a given bloodstain in a crime scene. This would be a significant benefit to the criminal justice community.

## I. Introduction

Crime scene reconstruction is the process of determining the events involved with a crime using the physical evidence present at the scene along with scientific methodology and deductive reasoning. Various techniques are used as part of this reconstruction process; including DNA evaluation, fingerprint identification, and the focus of this project, blood spatter analysis. In blood spatter analysis, the residual bloodstains left at the scene of a crime are used to determine the point of origin of a particular bloodletting event and the type of trauma that led to the bloodstain (e.g., gunshot, blunt force, sharp object, etc.) [1]. The determination of these factors assists crime-scene analysts in their efforts to establish the sequence of events that occurred during the crime.

Two typical bloodstains are shown in Figure 1. It is known that the size and shape of a bloodstain are caused by some of the physical conditions of the blood droplet at the point and time of impact and the roughness of the impact surface [2]. Stain size is quantitatively described as the area of the stain's circular or elliptical shape, whereas shape is quantified by the stain's aspect ratio as well as the number of spines and satellite drops around the stain contour [2] [3] [4] [5]. A spine is a disruption in the smooth periphery of a stain whereas a satellite drop is a small drop that has completely separated from the main droplet and has landed away from the main bloodstain, i.e., a small splash.

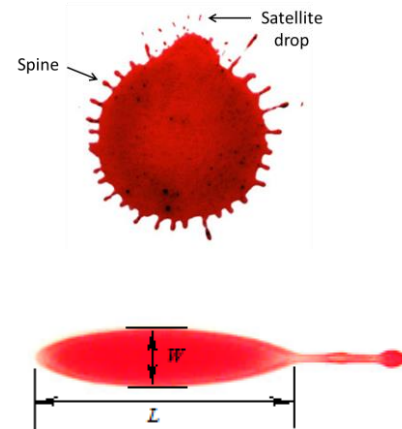


**Figure 1:** Typical bloodstain patterns. (Top) Near normal impact showing spines and satellite drops. (Bottom) Oblique impact to the right showing length and width measurements of the elliptical portion of the bloodstain.

Within this general framework of using the bloodstain size and shape to determine the blood droplet impact conditions, a number of different models and tools are used in the field [1] [6]. The use of specific correlations, strategies, software, etc. is dependent on the resources available to an examiner, which in turn are impacted by where and for whom the examiner works. As an example, the simplest technique is called stringing [2]. This method starts by using the aspect ratio of a bloodstain  $Ar$  to determine the impact angle  $\alpha$  of the blood droplet using the relation

$$\sin(\alpha) = W / L = Ar \quad (1)$$

where the impact angle  $\alpha$  is measured from the plane of the impact surface and the width  $W$  and the length  $L$  of the bloodstain are indicated in the bottom image in Figure 1. Balthazard, Piedelivre, Desoille and DeRobert [7] proposed this relationship in 1939 based on their experimental work, and it has become the predominant correlation in forensics analysis [2]. Using this relationship, a ray is typically drawn in a straight line from the stain in the direction of the angle  $\alpha$ . Repeating this process for a large number of individual droplet stains in a blood spatter pattern, the individual rays may converge in a nexus, or region of convergence. The point of origin of the bloodletting event is presumed to be this nexus. Additionally, under this method the speed of the droplet is determined by the size of the stain and the assumption that the volume of the blood droplet was “normal” [2], where a “normal” droplet is

defined as one containing 0.05 mL of blood [2]. This technique assumes that all stains are created by droplets of equal volume.

Recently, more refined methods have been developed in an effort to increase the accuracy of the results. Ballistics software has allowed for a more rigorous application of physics in determining droplet flight paths [1]. Using these tools, gravity, drag, and other forces acting on a droplet in flight may be taken into account. Correlations have also been developed that relate the number of spines to droplet impact speed [3] [4]. With these developments, the assumption of a droplet of “normal” volume is no longer required. Although these methods represent significant improvements over previous methods, they are still limited. A correlation is only valid for impacts within a certain range of impact conditions and for impacts on certain materials. Surface properties such as roughness, stiffness, and porosity affect spreading behavior and can either inhibit or promote spine and satellite formation [8] [9]. Thus, a more complete examination of the physics of droplet impacts may improve current blood stain examination techniques and lead to less ambiguity in the events surrounding crime-scene blood spatter analysis.

It is helpful in the discussion of droplet impact behavior to separate the droplet impact process into four stages: pre-impact, spreading, retraction, and final. Figure 2 illustrates the first three of these

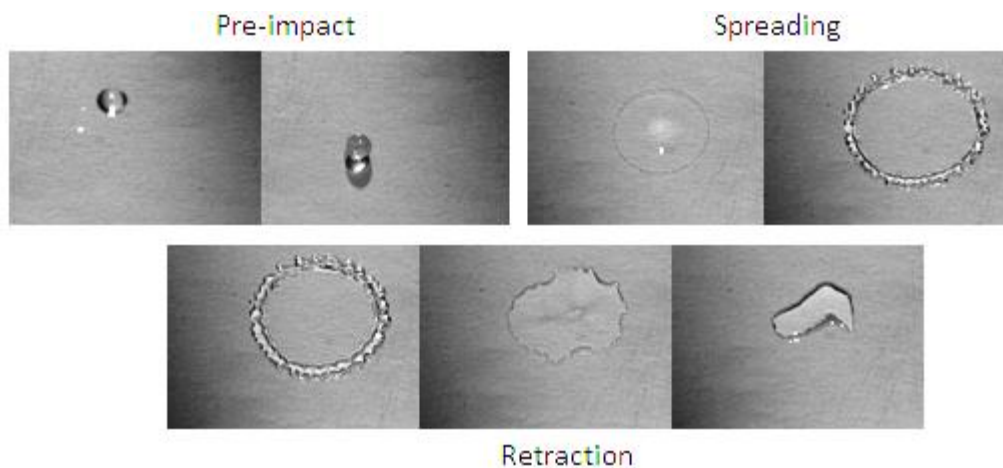


**Figure 2:** Illustration of droplet impact stages. This impact is for a 2.4 mm diameter water drop, traveling at 3.46 m/s, impacting glass at an angle of 70°. The Reynolds number is 7414. For each group of images, time increases from left to right. The surface slants downwards from left to right in every image.

stages. Pre-impact is the time after droplet generation but preceding the collision of the droplet with the surface. Here, the droplet is in free fall, gravity accelerates the droplet downward, the surrounding air exerts a drag force, and the droplet may experience oscillation due to its method of origination and/or the aerodynamic forces from flight. Impact signals the end of this stage and the beginning of the spreading stage. In this stage, the droplet spreads out along the substrate until the wetted area of the droplet on the substrate reaches a maximum, as shown in the top right image of Figure 2. Here, the liquid from the droplet is concentrated in a thick rim around the circumference of the droplet and there is a thin film of liquid inside the rim known as the lamella.

At this point of maximum spread the retraction process begins because the surface tension in the liquid rim pulls the rim back toward the center of the drop. The surface tension forces on the interface of the droplet must overcome the adhesive forces between the droplet and the solid surface for the retraction process to occur. Blood has a smaller surface tension than water and so on the same surface, water tends to retract while blood tends to remain in a fully spread state. This is shown in Figure 3 where there is noticeable retraction for an impact of a water droplet but almost no retraction during the impact of a liquid droplet with the fluid properties of blood.

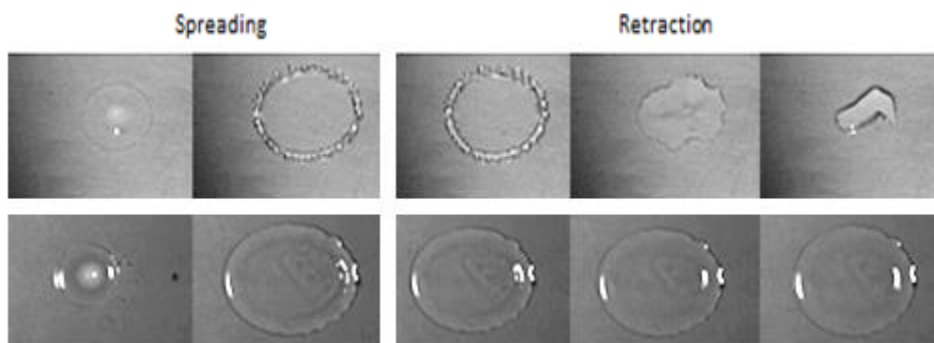


**Figure 3:** The spreading and retraction stages of droplet impact. (Top row) water at  $Re = 7400$ . (Bottom row) a blood simulant liquid at  $Re = 4000$ .

After the initial retraction of the droplet, the final stage of the droplet impact process is where the motion of the droplet is arrested by viscous dissipation and a final steady state shape is attained. During this stage, ambient conditions and the particular properties of the solid surface play greater roles than in the previous stages. For example, liquid can be wicked into the substrate material, it may begin to flow due to its own weight, and drying may inhibit the flow.

In the context of forensic science, a bloodstain is produced when blood from the impacting droplet penetrates, chemically reacts, or just adheres and dries onto the substrate material. The blood residue left behind on the substrate can be observed visually or with the help of chemicals such as luminol. Luminol mixed with an oxidizing agent such as hydrogen peroxide exhibits chemiluminescence when it reacts with the iron in hemoglobin, a protein in red blood cells, and it is the predominant chemical used in blood spatter analysis [10] [11]. The retraction stage is minimal for blood due to its lower surface tension and higher viscosity. The final stage as the droplet reaches steady state is affected by ambient conditions, such as temperature and humidity, and other factors such as wicking into the substrate material. However, these factors do not change the final shape of the bloodstain. Thus, the bloodstain is most affected by the spreading stage of droplet impact and this is exactly the process most affected by the impact properties of the droplet.

If the blood droplet did not penetrate, chemically react, or adhere to the solid surface, it would then eventually retract back into a static shape called a spherical cap with a circular contact line along the solid surface. In this case, the initial impact information would be lost except for the initial droplet size, which would correlate to the final diameter of the circular contact line on the solid surface. Part of any forensic analysis of blood spatter would be to recognize if the impact surface in question behaved in this

way. If not, there would be little point in proceeding further because most of the initial conditions of the droplet impact would be obscured.

In this project, the working definition for the shape of the bloodstain is that it corresponds to the region of maximum spreading of the droplet. Note that this initial region of droplet spreading is exactly where the process is most affected by the impact properties of the droplet and the properties of the solid surface.

The important physical parameters associated with the spreading stage of droplet impact are the droplet impact velocity  $V$ , diameter  $D$ , and impact angle  $\alpha$ ; and the fluid properties of density  $\rho$ , viscosity  $\mu$ , and surface tension  $\sigma$ . The properties of the solid surface, such as its average roughness, stiffness, wettability, and porosity are important in the details of the spreading process, but were not explored in detail in this project. The impact and fluid properties can be combined using dimensional analysis to produce two main dimensionless parameters, the Reynolds number  $Re$  and the Weber number  $We$ , defined as follows:

$$Re = \frac{\rho V D}{\mu}, \quad We = \frac{\rho V^2 D}{\sigma} \quad (2)$$

The Reynolds number is the ratio of inertial to viscous forces and the Weber number is the ratio of inertial to surface tension forces. In a crime scene situation where blood spatter may result from dripping, blunt-force trauma, or gunshot wounds, these dimensionless parameters fall into the following ranges [12]:

$$240 < Re < 6,000, \quad 20 < We < 2,100 \quad \text{dripping} \quad (3a)$$

$$10 < Re < 4,800, \quad 1 < We < 3,400 \quad \text{trauma} \quad (3b)$$

$$1 < Re < 12,000, \quad 1 < We < 85,000 \quad \text{gunshot} \quad (3c)$$

Note that the domains for dripping and trauma are almost the same at the high end, whereas the upper limit is much larger in a gunshot situation.

Some work on the role of fluid mechanics in the blood spatter problem has appeared in the literature. Adam [4] experimentally validated relationships between droplet size and velocity and the resulting stain size and the number of spines. He used stored human blood and focused specifically on droplet impacts on paper. For the range of droplet sizes and speeds tested, he concluded that there was a strong dependence of the number of spines and stain size on the impact speed. The majority of his work was focused on perpendicular impacts, but he performed a limited amount of work on inclined surfaces. He proposed the following relationship between the number of spines  $N$ , the impact angle  $\alpha$ , and the Weber number

$$N = We^{1/2} \sin(\alpha)^{7/2} \quad (4)$$

Carroll [13] also conducted droplet-impact research and her method of droplet generation was the starting point for the generator design used in this work. Carroll used a glycerin-water mixture for the droplets and similarly concluded that number of spines was dependent on the impact velocity. She also

found that the aspect ratio of the fully spread droplet on a surface was wildly unpredictable when comparing results obtained for different impact angles and materials. These results run counter to many standard practices in the forensics community and provided some motivation for the present work.

Finally, Hulse-Smith and Illes [3] used human blood to experiment with stain patterns on paper, wood, and drywall for perpendicular impacts. Based on their measurements, they developed two correlations relating the droplet impact diameter and velocity to the number of spines in the bloodstain and the diameter of the bloodstain  $D_s$

$$N = 146 \cdot DV^2 + 12.8, \quad \frac{D_s}{D} = 13.8 \cdot \sqrt[3]{DV}. \quad (5)$$

Using these two correlations, the impact diameter and velocity of a droplet of blood could be calculated from the observed number of spines and the bloodstain diameter. Hulse-Smith and Illes [3] neglected to include the physical properties of the blood in these correlations, arguing that since the properties of blood were the same for all impacts, the use of dimensional correlations was more practical. While true for their experiments, the physical properties of blood do influence the behavior of the droplet during spreading, and so this effect cannot be observed in the dimensional correlations of equation (5).

Although this previous work provides valuable insight into various aspects of droplet spreading behavior, many questions remain. Thus, the main goals of the present research program are as follows:

- a) quantify the effects of the droplet impact angle, the initial droplet size and speed, and the solid surface roughness and wettability on the pattern of the final observed stain defined by the point of maximum droplet spreading, and
- b) analyze these data to provide simplified, but relevant phenomenological models of droplet impact, spreading, and splashing that can be directly used by practitioners in the field of forensic science.

## II. Project Design and Methods

### 1) Experimental methods

The experimental facility designed for this work is shown in Figure 4. The primary components are a droplet generator, a target assembly, and a high-speed video camera. The droplet generator produces a single liquid droplet on demand with a specified size and speed directed vertically downward. The generator is mounted on a movable platform that can be positioned at a variable vertical distance to the target in order to increase the speed of the droplet using gravitational acceleration. The droplet impacts a solid surface held on the target assembly at a specified angle with respect to the vertical. The target assembly contains a pair of lasers and photodiodes used to measure the speed of the approaching droplet and a high-speed video camera used to observe and record the spreading of the droplet on the solid target surface.

The droplet generator can produce a single liquid droplet on-demand with various diameters and speeds. The generator has a liquid and an air chamber separated by a thin latex membrane as shown in Figure 5. To produce a droplet, the test liquid is allowed to flow into the liquid chamber until it is completely filled and all air bubbles are removed. The inlet and vent ports are then closed. A pressure pulse with a specified magnitude and duration is then used to inject air into the air chamber. The pulse is regulated by a pressure regulator and a solenoid valve and controlled by a LabView program. This pressure pulse determines the size and speed of the ejected droplet as it leaves the nozzle of the generator. The final impact speed of the droplet as it approaches the target surface is set by changing the height of the droplet generator above the target. The maximum height for this facility is 2.5 m, which is sufficient to reach terminal velocity of the droplet.

With this facility, single liquid droplets with diameters from 2–5 mm can be reliably and predictably produced. Droplet impact speeds can be as high as 5 m/s. In a forensics context, these droplets correspond to those created via dripping or some large droplet, low speed, blunt force trauma situations. Droplets resulting from gunshot wounds are typically much smaller and faster. However, the Reynolds and Weber number ranges covered in these experiments include both dripping and blunt force trauma situations.

A droplet produced by the droplet generator travels vertically downward until it strikes the target surface mounted on the target assembly shown in Figure 6. The target surface is mounted on a movable arm that can be positioned to orient the target at an arbitrary angle with respect to the vertical. The surface is

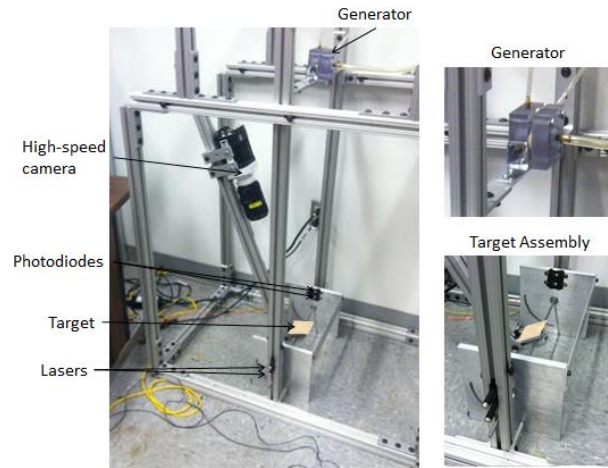


**Figure 4:** Experimental facility showing the droplet generator, the target assembly, the high-speed video camera, and the lasers and photodiodes.

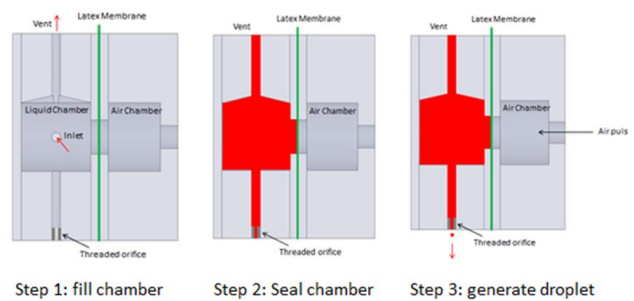


**Figure 5:** Operation of the droplet generator. Step 1) Fill the liquid chamber with test liquid. Step 2) Close the inlet and vent ports. Step 3) Inject a well-defined air pulse into the air chamber to deflect the latex membrane and produce a desired droplet.

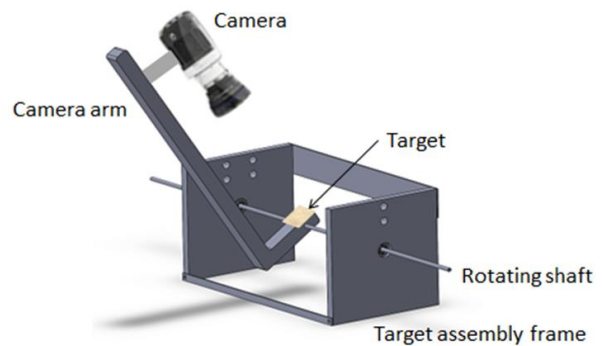


**Figure 6:** Target assembly with interchangeable target surfaces, mounting holes for the lasers and photodiodes, and a high-speed video camera.

interchangeable to allow different surfaces to be investigated and prepared prior to each experiment. The impact speed of the droplet is measured by a pair of parallel laser beams held a fixed distance apart, aligned with the path of the droplet, and monitored with a pair of photodiodes. As the droplet passes through each laser beam the current output of each photodiode is interrupted from which the passage time of the droplet and hence the impact velocity is measured.

Three different target surfaces were used during this research: glass, bathroom tile, and paper. The glass and tile surfaces were thoroughly cleaned prior to each test. A fresh piece of paper was used for each test when paper was the target surface. The roughness of these surfaces was measured using a standard surface profilometer and the results for each surface are given in Table 1. The roughness is the same in all directions for the glass and tile surfaces. However, the paper surface has a directional dependence as indicated in the caption of Table 1.

| <i>Material</i>                 | glass | tile | paper   |
|---------------------------------|-------|------|---------|
| $\varepsilon$ ( $\mu\text{m}$ ) | 2.0   | 48.  | 224/292 |

**Table 1:** The measured roughness of the three types of target surfaces used in this research. The roughness  $\varepsilon$  is defined as the average deviation of the absolute value of the surface profile about the mean. The roughness of the paper surface depended on the direction along the surface. The first value is along the direction of travel of the droplet when it strikes the surface. The second larger value is for the transverse direction.

The primary data of interest in these experiments is the spreading behavior of the droplet as it spreads along the target surface. Images of this process were recorded using a Phantom Miro M120 high-speed video camera mounted on the same movable arm as the target (see Figures 4, 6). The camera is held above the target surface and the movable arm ensures that the view angle of the camera is always  $90^\circ$  (normal) with respect to the plane of the surface even when the target surface is inclined.

Finally, the initial droplet diameter assuming a spherical droplet was obtained by measuring the mass of the target surface before and after each droplet impact. A Mettler AE160 analytical balance was used for this measurement.

## 2) Blood simulant

Blood is both a viscoelastic and shear thinning fluid. However, for shear rates larger than  $100 \text{ s}^{-1}$ , which are typical in the droplet impact events seen in this experimental facility, it behaves as if it were a Newtonian fluid [18]. Thus, to simplify the experimental procedures a blood simulant was developed based on a mixture of water, glycerin, and alcohol. The resulting mixture matched the kinematic viscosity of blood at 4.15 cSt and the surface tension of blood at 62 mN/m as shown in the property curves of the mixture in Figure 7. Due to the temperature-dependent nature of the viscosity of water-glycerin mixtures, ambient

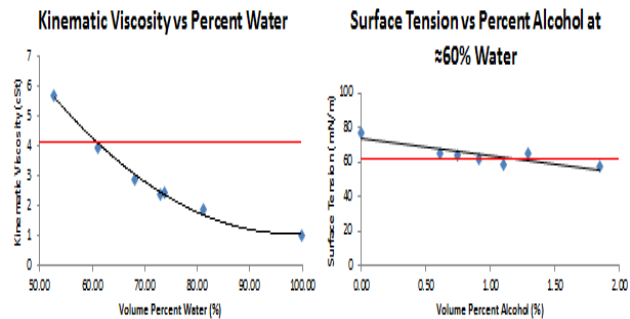


**Figure 7:** Blood simulant property curves versus volume percent of water and alcohol. The red line indicates the desired properties of blood.

conditions were carefully monitored to ensure that test conditions and liquid properties were maintained at constant values. The simulant liquid was prepared and tested before each experimental run to verify that the properties were correct. The viscosity was measured using a Cannon-Fenske Routine viscometer, the surface tension was measured using the pendant-drop method [14], and the density was measured by weighing a sample of a given volume on the Mettler AE160 analytical balance. Assuming a temperature change of 0.5 °C, the relative uncertainty in the Reynolds number calculation for the blood simulant increased from 3.7% to 4.0% and the uncertainty in the Weber number did not change from 6.8%. Thus, this temperature effect was safely ignored.

Note that using a Newtonian blood simulant also provides a good baseline study from which the non-Newtonian effects of blood can be explored in a later project.

### 3) Numerical methods

The numerical simulation of the droplet impact problem was designed from scratch using modern computing techniques optimized for parallel processing on a graphic processing unit (GPU). The 3-D time dependent simulation uses the fluid-flow governing equations for mass, momentum, and energy written in compressible form since this formulation is *ideally suited for GPU parallelization*. Air was treated as an ideal gas and an appropriate equation of state for liquid compressibility was used. The interface of the droplet was modeled using the level-set method. The spatial discretization of the equations is based on a fourth-order finite difference scheme with a wavelet adaptive multi-resolution grid to automatically resolve and capture the fine length scales of the motion as the system evolves in time.

For fully compressible flows, a variety of explicit time integration methods can be selected by the user to evolve the governing equations in time. In the droplet impact problem, the effect of compressibility is very small in the liquid, but is important in the gas layer underneath the droplet [19, 20]. This is addressed in the wavelet simulation through the use of a new implicit dual-time stepping scheme that integrates the acoustic pressure field on an extremely fast time scale to compute the bulk pressure experienced by each fluid as it moves. The net effect of the fast acoustic field is to maintain an incompressible flow in the domain of the liquid, i.e., no volume change in the liquid, while allowing for compressibility effects in the gas layer underneath the droplet. Thus, *this GPU simulation with dual time stepping will compute an incompressible flow field in the liquid even though the equations are written in compressible form*. Details of this simulation can be found in Forster [17].

### 4) Data analysis

At the beginning of each test, the density  $\rho$ , viscosity  $\mu$ , and surface tension  $\sigma$  of the blood simulant were measured. The angle of impact  $\alpha$  of the droplet (defined in Figure 8) was set on the experimental facility. A droplet was then generated and its impact velocity  $V$  was measured with the laser/photodiode sensors. The initial droplet diameter  $D$

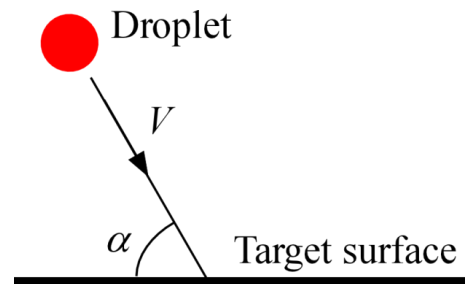


**Figure 8:** Sketch of droplet impact defining the angle of impact.

based on an initial spherical droplet was determined by weighing the target before the test, weighing the droplet on the target after the test, and using the known density of the liquid.

These dimensional parameters are combined using dimensional analysis to form two dimensionless parameters: the Reynolds number  $Re$  and the Weber number  $We$ , defined in equation (2). In the present experiments, these parameters vary over the ranges:

$$1,200 < Re < 5,400, \quad \text{and} \quad 240 < We < 1,920. \quad (6)$$

These values are a subset of the ranges typically seen in forensics problems, shown in equations (3) and are typical of dripping and some blunt trauma situations.

The high-speed video camera records the motion of the droplet as it impacts and spreads along the target surface. Of particular interest to the bloodstain problem is the shape of the droplet on the solid surface at its maximum extent, since this is the present definition of the stain left by a blood droplet on the target surface. An example of such a shape is shown in Figure 9. Here, a droplet of blood simulant has spread to its maximum extent on a glass surface at an impact angle of  $40^\circ$ . The droplet was moving from left to right in the image. The current practice in forensics bloodstain pattern analysis is to fit an ellipse to this shape as illustrated in Figure 9. The primary measurements of this maximal shape are the width  $W$  and length  $L$  of the ellipse and the number of spines along the periphery of the droplet. The aspect ratio of the ellipse is computed using the relation from equation (1), i.e.,

$$Ar = W/L. \quad (7)$$

The current practice in bloodstain pattern analysis is to use the measured aspect ratio of the ellipse to determine the angle of impact of the blood droplet  $\alpha$  using the formula

$$\sin(\alpha) = Ar \quad (8)$$

One of the concerns of this research is to evaluate the accuracy of this common approach.

Another measure of the impact process is the spreading factor  $S_f$ , defined as the planar area of the elliptical shape of the stain over the cross-sectional area of the drop. Thus,

$$S_f = \frac{\pi LW / 4}{\pi D^2 / 4} = \frac{LW}{D^2}. \quad (9)$$

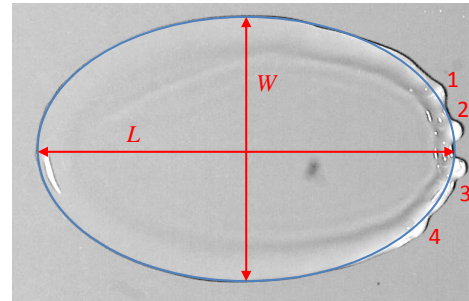


**Figure 9:** A droplet of blood simulant at its point of maximum spreading on a glass surface at an impact angle of  $40^\circ$ . The droplet was moving from left to right. Also shown is the blue-grey ellipse fitted to the shape of the spreading droplet. In this case, four spines occur on the leading (right) edge of the droplet.

### III. Results

#### 1) Experimental work

The experimental facility described above was used to perform 182 experiments with three different target surfaces: 78 on clean glass, 52 on bathroom tile, and 52 on paper. Typical results from these experiments are shown in Figure 10 for droplet impact on a tile surface for various impact angles and Reynolds numbers. For this range of Reynolds numbers, the stain aspect ratio is almost constant with Reynolds number for most impact angles. A small increase in the aspect ratio as the Reynolds number increases is observed for an impact angle of 30°. Figure 11 shows the aspect ratio versus the angle of impact for all Reynolds numbers and glass, tile, and paper surfaces. This figure shows that the common practice relation is fairly accurate for near normal impact angles, but that it would under-predict the impact angle for a given bloodstain aspect ratio for oblique angles less than about 40°.

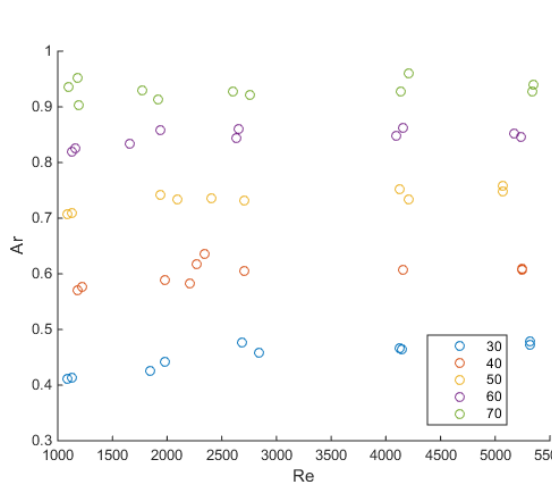


**Figure 10:** The aspect ratio of a bloodstain on a tile surface versus the Reynolds number for various impact angles.

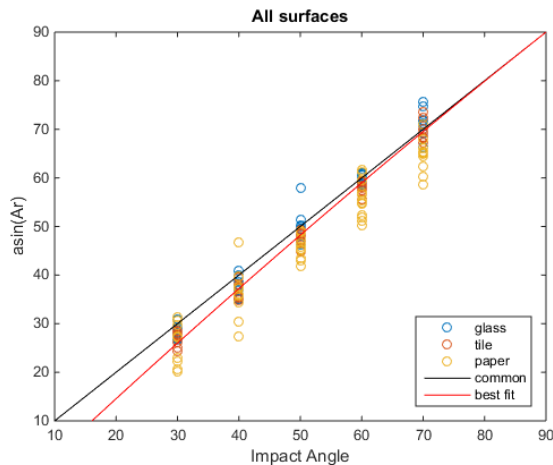


**Figure 11:** The arcsin of the aspect ratio of a bloodstain versus the impact angle in degrees for all surfaces and Reynolds numbers. The solid black line is the common practice relationship and the red line is the best fit curve of equation (10).

The data from Figure 11 were fitted in a least-squares sense to a new curve based on the common practice relation with the form

$$\alpha = x + c \{90^\circ - x\}^2, \quad x = \text{asin}(Ar), \tag{10}$$

where  $x$  is an angle expressed in degrees. Here,  $x$  is the predictor or independent variable and  $\alpha$  is the response or dependent variable. A comprehensive fit to all the data in Figure 11 gives  $c = 1/898$ . For reference, the values of the fitting constant  $c$  for all of the materials separately are shown in Table 2. The fourth column of this table gives the goodness-of-fit of equation (10) to the data for each material as measured by the coefficient of determination  $R^2$ . This coefficient gives the amount of the variation of the data captured by the model equation. For these data, the fit is very good. Note that is also better

that the corresponding fit of the data to the common practice relation of a straight line, given in the fifth column of Table 2.

The relative uncertainty in the parameter  $\text{asin}(Ar)$  used in Figure 11 can be estimated based on the uncertainties in the measurements of the bloodstain length and width. When  $\alpha = 70^\circ$ , this relative uncertainty is about 6% and for  $\alpha = 30^\circ$ , it is about 10%. The total relative variation in the data about the mean that is present in Figure 11 is 13% for  $\alpha = 70^\circ$  and 22% for  $\alpha = 30^\circ$ . Thus, the relative variation in the data is about twice the uncertainty in the data. For this reason, the measurement error is assumed to be contained in the total variation of the data and not specifically mentioned in any of the subsequent statistical error analyses.

The experimental data was also analyzed using ideas from Eggers *et al.* [15]. In that work, normal droplet impact was considered and it was shown that the maximum spreading diameter was governed by the transfer of the kinetic energy of the droplet to capillary energy (surface energy of the fully spread droplet) with some energy dissipation through a viscous boundary layer on the solid surface. Eggers *et al.* [15] formulated a relationship between the problem parameters that also holds in the present droplet impact problem. Here, the width of the spreading droplet in the lateral direction and the normal component of the impact velocity were used. The relationship is given by

$$W_r Re_n^{-1/5} = \frac{c_1 P^{1/2}}{c_2 + P^{1/2}}, \quad P = We_n Re_n^{-2/5}, \quad (11)$$

where  $W_r = W_{\max} / D$  is the dimensionless maximum lateral spreading width of the droplet,  $Re_n = \rho V_{\text{norm}} D / \mu$  is the Reynolds number based on the normal impact velocity  $V_{\text{norm}}$ ,  $We_n = \rho V_{\text{norm}}^2 D / \sigma$  is the Weber number based on the normal impact velocity, and the constants  $c_1$  and  $c_2$  are used to fit the data. Here,  $We Re_n^{-2/5}$  is the predictor or independent variable and  $W_r Re_n^{-1/5}$  is the response or dependent variable. Figure 12 shows the fitting result for all surfaces. The red curve is equation (11) with a fit to all of the present data of  $[c_1, c_2] = [1.01, 1.07]$ . The coefficient of determination of this fit is  $R^2 = 0.342$ , which is

| Material | $c$     | $1/c$ | $R^2 (10)$ | $R^2 (cp)$ |
|----------|---------|-------|------------|------------|
| Glass    | 6.71e-4 | 1490  | 0.982      | 0.970      |
| Tile     | 1.06e-3 | 941   | 0.984      | 0.952      |
| Paper    | 1.72e-3 | 583   | 0.915      | 0.819      |
| All data | 1.11e-3 | 898   | 0.958      | 0.923      |

**Table 2:** The constant  $c$  in the fitting function of equation (10) for each of the materials used in this experiment. The column  $R^2 (10)$  is the coefficient of determination for the fit of equation (10). The column  $R^2 (cp)$  is the coefficient of determination for the fit to the common practice relation,  $\alpha = \text{asin}(Ar)$ .

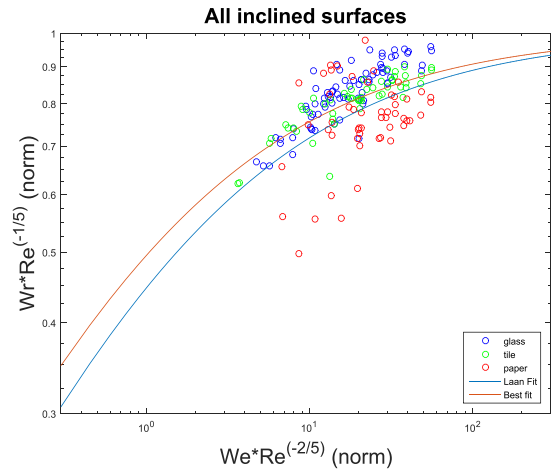


**Figure 12:** The experimental data for lateral droplet spreading normalized as shown in equation (11). The solid red line is the fit to equation (11) for the data on all surfaces. The lower, solid blue line is the fit to the results of the normal impact experiments in Laan *et al.* [16].

expected because of the large variation of the data seen in Figure 12. Also shown is a blue curve which is the fit obtained by Laan *et al.* [16] for normal droplet impact on a variety of surfaces of  $[c_1, c_2] = [1, 1.24]$ . While the present data do not have a very large range in this parameter space, they still seem to be reasonably close to the expected fit from Laan *et al.* [16]. It is also clear that there is a dependence of the spreading width on the type of surface.

Another parameter of interest is the eccentricity ratio of the bloodstain, defined as

$$Ec = (L - W) / D \tag{12}$$

The eccentricity parameter can be scaled in a similar way to that shown in equation (11) to reflect the spreading physics involved. However, one difference is a factor of  $\cos(\alpha)$  used to include the effect of the inclination angle on the longitudinal spreading of the droplet. As  $\alpha$  approaches  $90^\circ$  (normal impact), the eccentricity  $Ec$  should approach zero. This

normalized parameter,  $Ec \cdot Re_n^{-1/5} / \cos(\alpha)$ , is plotted in Figure 13. The black line is a linear, least-squares fit to a straight line for all of the data. It has a slope of -0.014 and a y-intercept of 0.83. Here,  $We Re_n^{-2/5}$  is the predictor or independent variable and  $Ec \cdot Re_n^{-1/5} / \cos(\alpha)$  is the response or dependent variable. The coefficient of determination of this fit is  $R^2 = 0.307$ . In this plot, the data for all of the surfaces and all of the inclination angles have at least collapsed into a single region spread out about the fitting line. This suggests that the scaling may have captured some of the appropriate physics. However, more data are needed to investigate the variability seen in the present results.

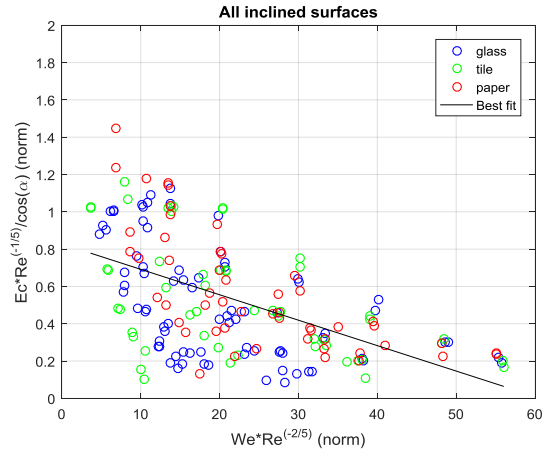


**Figure 13:** The eccentricity ratio for droplet spreading normalized as shown in equation (11). The solid black line is a linear, least-squares fit for all data on all surfaces.

Figure 14 is a plot of the spreading factor on a tile surface versus the impact angle for various Reynolds numbers. These data show that the impact angle only weakly influences the spreading factor, but that the effect increases as the Reynolds number increases. Using the same kind of scaling ideas as above, the spreading factor has a functional relationship as shown in equation (13)

$$S_f Re^{3/10} = f(We Re^{-2/5}) \tag{13}$$

The present data for all surfaces is scaled in this way and plotted in Figure 15. The black line in the figure is a linear, least-squares fit to all of the data. It has a slope of 4.6 and a y-intercept of 96. Here,  $We Re_n^{-2/5}$  is the predictor or independent variable and  $S_f Re_n^{3/10}$  is the response or dependent variable. The coefficient of determination of this fit is  $R^2 = 0.517$ . These results have a better fit than the data for the eccentricity, although it is still not very good. There also appears to be a slight surface effect with some of the results for paper being smaller than those for glass.

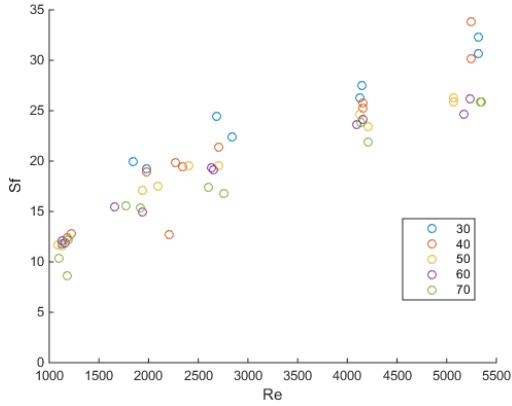


**Figure 14:** The spreading factor of a bloodstain on a tile surface versus Reynolds number for various impact angles.

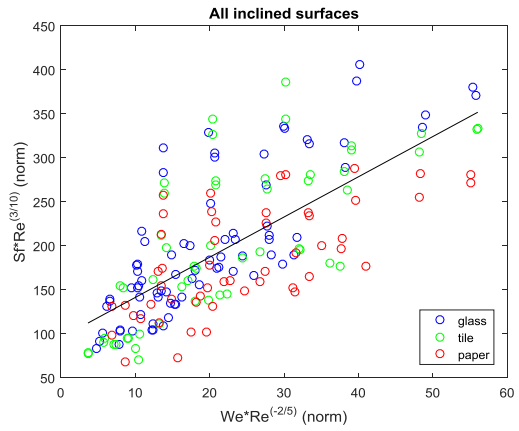


**Figure 15:** The experimental data for spreading factor normalized as shown in equation (13). The solid black line is a linear, least-squares fit for all data on all surfaces.

When the impact velocity of the droplet is large enough, spines and/or satellite droplets can appear as shown in Figures 1 and 9. This indicates either the start or the presence of splashing. In the present experiment, the number of spines was counted and the data are plotted in Figure 16 using the same scaling as in equation (11). The lines in this figure are a linear, least-squares fit to the data for each

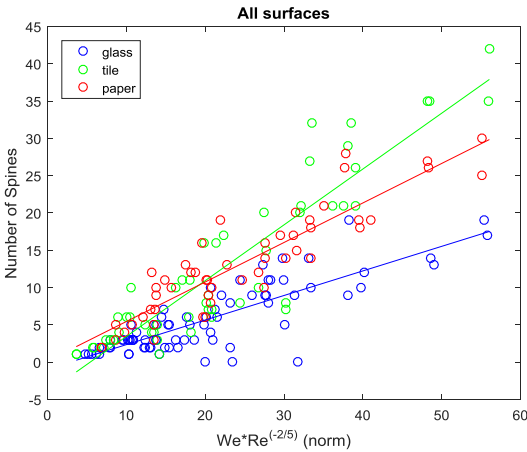


**Figure 16:** The experimental data for the number of spines plotted using the scaling shown in equation (11). The solid lines are a linear, least-squares fit for the data on each surface.

| Material | $c_1$ | $c_2$  | $R^2$ |
|----------|-------|--------|-------|
| Glass    | 0.329 | -0.943 | 0.693 |
| Tile     | 0.748 | -4.037 | 0.842 |
| Paper    | 0.530 | 0.156  | 0.824 |

**Table 3:** The results of the linear least squares fit to the data of Figure 16. The fitting line is  $y = c_1x + c_2$ . The two constants for this fit are shown in columns 2 and 3 for each material. The column  $R^2$  is the coefficient of determination for the fit of this equation.

material separately. For each line,  $We Re_n^{-2/5}$  is the predictor or independent variable and the number of spines is the response or dependent variable. The detailed results of these fits are shown in Table 3. This shows a clear effect of the type of surface on the number of spines that appear during spreading. However, the effect is not as straightforward as one might imagine. The glass surface is the smoothest and it has the fewest spines. The next smoothest surface is tile and it seems to have more spines than the roughest surface, which is paper. The surface roughness affects the spreading of the droplet and the subsequent instability of the droplet rim. For paper, there may also be an effect of absorption of the

liquid into the paper. The mechanisms of these interactions are not clear and need to be studied in future work.

Eggers *et al.* [15] also proposed a simple model for droplet spreading on a solid surface with a normal impact velocity. The model is based on the bulk acceleration of the droplet rim driven by a stagnation point flow in the thin film of liquid near the droplet center. In this thin film there is also a boundary layer flow that eventually arrests the stagnation point flow. The results of their model compared well to their own numerical simulations of axisymmetric, normal droplet impact.

This model was investigated and improved in several ways in the present work. The results for one case of normal droplet impact with  $Re = 1807$  and  $We = 320$ , which is appropriate to blood spatter, is shown in Figure 17. This model seems to be quite successful for normal impact as it follows the numerical simulations of Eggers *et al.* [15] for normal droplet impact and spreading. It seems likely that it can be extended to the situation of oblique droplet impact that is of relevance to blood spatter.

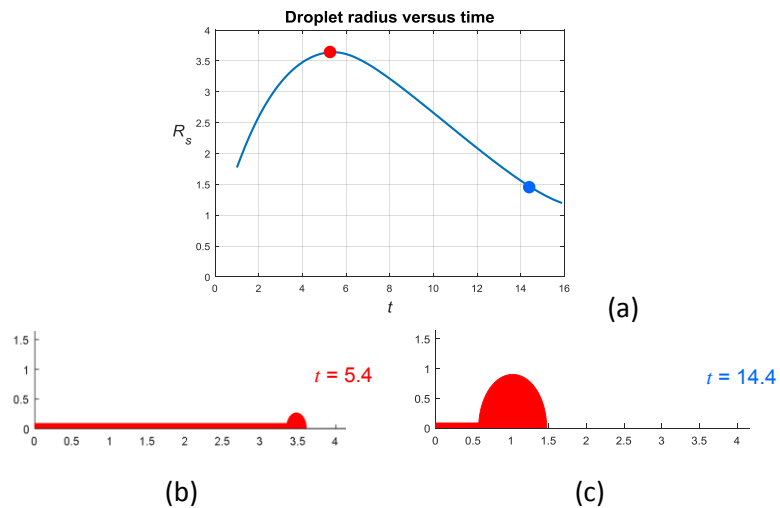


**Figure 17:** A numerical model of normal impact droplet spreading using the ideas of Eggers *et al.* [15]. Here,  $Re = 1807$  and  $We = 320$ . (a) is the time history of the normalized droplet radius, (b) is the droplet shape at maximum spreading, and (c) is the droplet shape just before full retraction.

## 2) Numerical work

The GPU-based, wavelet-adaptive, 3-D, multiphase flow simulation was only partially completed during this project. The level-set model for a multiphase flow was not finished during the time frame of this project. At present, the simulation can only solve for single phase flow fields under compressible and/or incompressible flow conditions. The wavelet grid allows it to provide fully resolved flow fields and the GPU programming provides extremely fast execution speeds. These capabilities are demonstrated in the following two example simulations.

The first example is a compressible flow; the classic Richtmyer-Meshkov instability on a circular bubble in 2-D as shown in Figure 18. Here, a circular gas bubble is struck by a normal shock wave traveling from left to right in the figure. The shock wave (now located to the right of the bubble at the dark-orange/green

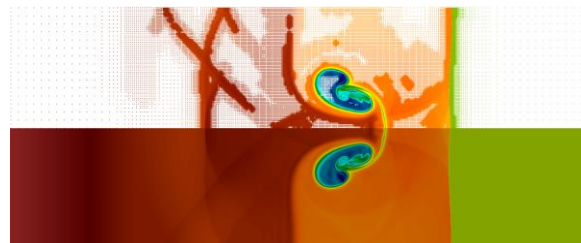


**Figure 18:** The density field in the Richtmyer-Meshkov instability arising from a 2-D, viscous, shock-bubble interaction. The top portion of the plot shows the wavelet-adaptive point representation of the density and the bottom shows the reconstructed density field on a uniform grid.

boundary) causes the bubble to roll-up and break into two pieces that follow the shock wave as shown. Similar results are also seen in 3-D.

A popular benchmark incompressible flow example is the flow in a 2-D, lid-driven cavity. In this system, the top wall of the cavity moves to the right at a constant speed and the remaining three walls are stationary. The resulting flow is a clockwise vortex in the cavity as shown in Figure 19. The flow is considered incompressible since the Mach number, the ratio of the flow speed to the sound speed, is always less than 0.001 in this flow domain. Compressible effects start to become important in a flow when the Mach number is larger than about 0.3. This problem highlights the simulation's ability to solve for an incompressible flow even though the governing equations used in the simulation are the compressible flow equations.

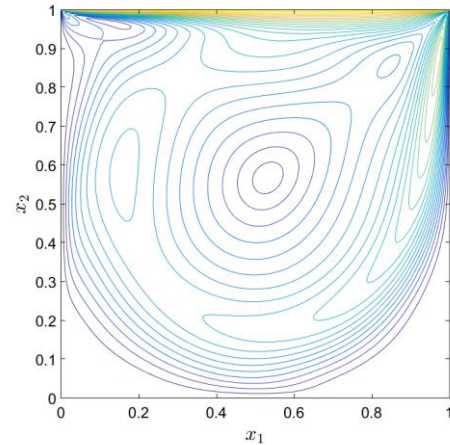


**Figure 19:** Contours of velocity magnitude in a lid-driven cavity flow for  $Re = 1000$  and  $Ma = 0.001$ . The top wall is moving to the right and all other walls are stationary.

## IV. Conclusions

### 1) Discussion of findings

The experimental findings shown in Figure 11 demonstrate that the common practice relation between the droplet impact angle and the bloodstain aspect ratio, i.e.,  $\sin(\alpha) = Ar$ , is in significant error for shallow impact angle less than about  $40^\circ$ . A new correlation to correct this error is given in equation (10). The correlation was fitted to all of the data and to each surface type individually, with the results given in Table 2. These results show that the correction is greater for rougher surfaces, i.e., rougher surfaces produce smaller aspect ratios for the final bloodstain. Note that these results are also limited to a forensic parameter range typical of either dripping or blunt force trauma situations.

The mechanistic ideas discussed in the work of Eggers *et al.* [15] indicate that the maximum droplet spreading normal to the impact vector is governed by the transfer of the kinetic energy of the droplet to capillary energy (surface energy of the fully spread droplet) with some energy dissipation through a viscous boundary layer on the solid surface. Figure 12 shows that when the experimental data are scaled using appropriate scaling parameters that reflect this balance the result is a collapse near a representative curve that compares well to the curve from Laan *et al.* [16]. Again, the roughness of the surface does appear to have some influence with rougher surfaces decreasing the lateral spreading of the droplet.

Three other parameters were plotted using these same ideas; the eccentricity ratio in equation (12), the spreading factor from equation (9), and the number of spines on the droplet periphery. These results are shown in Figures 13, 15, and 16. The eccentricity ratio and the spreading factor seem to have collapsed into a single region, but there is still significant variability in the data. The results shown in Figure 14 for the spreading factor indicates that this variability is not due to variations in the impact angle. The results for the number of spines do collapse into a single curve for small values of the

parameter  $P$  as defined in equation (11). However, there is a significant surface roughness effect as  $P$  increases.

A primary limitation of this work is the variability seen in all of the data, which may be a result of how the droplets were generated. Any method of droplet generation will cause some droplet oscillations. If these oscillations are not damped out before the droplet strikes the surface, the deformed shape of the droplet may affect the spreading process. Another effect may be variable surface roughness. The tile and paper surfaces used do not have the same roughness, and furthermore, the roughness may not even be distributed uniformly over the surface. Even for the smooth glass surface, it is known that contamination can affect the droplet spreading process. To verify the source of the data variability, the experiments need to be repeated with more careful control or at least better characterization of the droplet generation process. There should also be better control on the uniformity and magnitude of the roughness of the impact surfaces. It would also be useful to have a larger number of impact surfaces covering a wider range of roughness magnitude.

The phenomenological model for the normal impact of a droplet described by Eggers *et al.* [15] is based on the idea that the droplet rim is accelerated outward by a stagnation point flow produced by the impacting droplet. The results for an improved version of this model are shown in Figure 17. These results compared well with the numerical simulations of droplet spreading by Eggers *et al.* [15] and seem to do a good job of predicting the maximum spreading diameter of the droplet.

The GPU-based, wavelet-adaptive, 3-D, flow simulation was completed during this project for single phase flows. The simulation was verified against a number of well characterized benchmark flow problems, including compressible flows and incompressible flows. The comparisons were excellent, with the simulation's resolution self-adapting to the flow conditions to meet a user-specified error tolerance.

However, the wavelet multiphase flow simulation was not completed during the time frame of this project. The inclusion of the level set model and its application to the droplet impact problem will be the subject of the future work discussed below.

## **2) Implications for policy and practice**

Bloodstain pattern analysis is an important tool in the criminal justice community. The bloodstain problem of interest to this research is the impact of a blood droplet on a solid surface. The final bloodstain on the surface is the result of very complex fluid dynamical processes involved in the spreading and splashing of the droplet. Thus, it is not surprising that the current simple relations used to predict the droplet impact velocity and angle from the appearance of the final bloodstain do not work well in all cases.

The results of this research have produced a new set of simple correlations for use in bloodstain pattern analysis. From the normal measurements of the length and width of a bloodstain, this work has produced a correction to the standard practice relation used to compute the impact angle of the blood droplet. The correction is significant for shallow impact angles of less than about 40°. These results also showed that this correction depends on the roughness of the surface, with rougher surfaces having a

larger correction. This work also developed two correlations, one for the lateral spreading of the bloodstain and one for the eccentricity of the bloodstain that can be used with the correlation for the impact angle to determine the impact speed and diameter of the blood droplet. However, these predictions have significant error because of the variability of the data used for the correlations. If this variability can be quantified in some way as discussed in the next section, it is expected that the use of these correlations would allow for a more accurate assessment of the initial conditions related to a given bloodstain in a crime scene. This would be a significant benefit to the criminal justice community.

### 3) Implications for further research

The experimental results discussed above imply three main areas for future work. First, the scaling used in equation (11) produced the parameter  $P = We_n Re_n^{-2/5}$ , which was the main independent variable used to plot the data. Figure 12 shows that this worked reasonably well, but that the bulk of the present data fell in the range between the two scaling limits of this parameter, i.e., very small  $P$  and very large  $P$ . This parameter written in terms of primitive parameters is  $P = (\rho\nu^{2/5} / \sigma) V_n^{8/5} D^{3/5}$ , where  $\nu$  is the kinematic viscosity of the fluid. Thus, to address these two limits, experiments should be performed for blood simulant droplets that are both smaller and slower, and larger and faster.

The next two areas of future work are concerned with the variability seen in the present data. This research used glass, tile, and paper surfaces as representative of what would be seen in a typical crime scene. The results showed a significant effect of surface roughness on the droplet spreading process, the shape of the fully spread droplet, and the onset and number of spines. This effect can be explored and characterized with another set of experiments using surfaces of well-defined and uniform roughness. The surfaces can be made from etched glass and range from completely smooth to as rough as needed to explore the effect on spreading and splashing of the impacting droplets. The use of glass would eliminate any effects that could be attributed to a porous surface such as paper.

The last area of experimental research is to examine the effect of droplet oscillations on the results. This is essentially a study of how the shape of an oscillating droplet just before impact affects the way the droplet spreads on the surface. This could be accomplished by acoustically forcing the droplet so that it oscillates in one of its fundamental modes of oscillation. The shape of the droplet just before impact could then be controlled by the acoustic signal to adjust the phase and amplitude of the droplet deformation to the desired point.

These last two studies on the variability of the data using controlled droplet oscillations and surface roughness are very important with respect to the use of this work in forensics applications. At a crime scene, there is no control of either of these parameters. Thus, if these future studies can adequately quantify the effect of each of these parameters on the size and shape of the bloodstain, then these results can be used to estimate to expected error in the computation of the impact parameters for use in forensics.

The GPU-based, wavelet-adaptive, single phase flow simulation was completed and verified in this project. The future work with this simulation will be to add the level set model for the simulation of

multiphase flows. Once completed and verified, the simulation will be used for a comprehensive parameter study of droplet impact on an inclined solid surface with arbitrary roughness as appropriate to the blood spatter problem and a comparison of those simulations to the experimental results obtained in this project. This will include a closer examination of the dependence of the aspect ratio, the width ratio, the eccentricity ratio, and the spreading factor of the bloodstain on the Reynolds number, Weber number, and impact angle of the blood droplet, and the roughness of the surface. These simulations would also enable a detailed investigation of the physical mechanisms associated with droplet impact and how these mechanisms are affected by droplet deformation due to initial oscillations and the friction attributed to surface roughness.

The fully resolved numerical simulation of droplet impact can also be used to more fully verify the simple droplet spreading model of Eggers *et al.* [15]. The verified normal impact model could then be extended in future work to produce an oblique droplet impact and spreading model. This would be a set of partial differential equations that describe the shape and spreading of a droplet on a solid surface. Using the idea that the maximum spreading of the droplet is the shape of the bloodstain, these equations would allow a quick determination of the shape of a bloodstain as a function of the droplet impact angle and speed, the droplet size and its physical parameters such as viscosity and surface tension, and the amount of surface roughness. The results from this model would be compared and validated against the experimental data on droplet shape and spreading factor and against the data from the fully resolved numerical simulation of droplet spreading.

The results from this simple phenomenological model of droplet spreading verified by the fully resolved numerical simulations would assist in the development of simple correlations or computations that could be used by forensic practitioners in the field. These results would be fully justified on scientific grounds and have a rational measure of expected error. Their use in forensics would greatly enhance the ability of practitioners to reconstruct a crime scene based on the available blood spatter evidence.

## V. References

- [1] U. Buck, B. Kneubuehl, S. Nather, N. Albertini, L. Schmidt, and M. Thali, "3D Bloodstain Pattern Analysis: Ballistic Reconstruction of the Trajectories of Blood Drops and Determination of the Centres of Origin of the Bloodstains," *Forensic Science International*, vol. 206, no. 1-3, pp. 22-28, 2011.
- [2] P. A. Pizzola, S. Roth, and P. R. D. Forest, "Blood Droplet Dynamics," *Journal of Forensic Sciences*, vol. 31, no. 1, pp. 36-49, 1986.
- [3] L. Hulse-Smith and M. Illes, "A Blind Trial Evaluation of a Crime Scene Methodology for Deducing Impact Velocity and Droplet Size from Circular Bloodstains," *Journal of Forensic Sciences*, vol. 52, no. 1, pp. 65-69, 2007.
- [4] C. D. Adam, "Fundamental Studies of Bloodstain Formation and Characteristics," *Forensic Science International*, vol. 219, no. 1-3, pp. 76-87, 2012.

- [5] C. Knock and M. Davison, "Predicting the Position of the Source of Blood Stains for Angled Impacts," *Journal of Forensic Sciences*, vol. 52, no. 5, pp. 1044-1049, 2007.
- [6] M. Boue and M. Illes, "Robust Estimation for Area of Origin in Bloodstain Pattern Analysis via Directional Analysis," *Forensic Science International*, vol. 226, no. 1-3, pp. 223-229, 2013.
- [7] V. Balthazard, R. Piedelievre, H. Desoille, and L. DeRobert, "Study of projected drops of blood," *Ann Med Leg Criminol Police Sci Toxicol*, vol. 19, pp. 265-323, 1939.
- [8] J. C. Bird, S. S. Tsai, and H. A. Stone, "Inclined to Splash: Triggering and Inhibiting a Splash with Tangential Velocity," *New Journal of Physics*, vol. 11, no. 6, 2009.
- [9] K. Range and F. Feuillebois, "Influence of Surface Roughness on Liquid Droplet Impact," *Journal of Colloid and Interface Science*, vol. 203, pp. 16-30, 1998.
- [10] A. Costello, F. Fances, and F. Verdu, "Bleach interference in forensic luminol tests on porous surfaces: More about the drying time effect," *Talanta*, vol. 77, no. 4, pp. 1555-1557, 2009.
- [11] B. Karger, S. Rand, T. Fracasso, and H. Pfeiffer, "Bloodstain Pattern Analysis-Casework Experience," *Forensic Science International*, vol. 181, no. 1-3, pp. 15-20, 2008.
- [12] D. Attinger, C. Moore, A. Donaldson, A. Jafari, and H. A. Stone, "Fluid Dynamics Topics in Bloodstain Pattern Analysis: Comparative Review and Research Opportunities," *Forensic Science International*, vol. 231, no. 1-3, pp. 375-396, 2013.
- [13] P. L. Carroll, "Results Obtained from Planar-Impact Experiment," Summer Research Project, Georgia Institute of Technology, 2010.
- [14] J. Andreas, A. Hause, and W. Tucker, "Boundary Tension by Pendant Drops," in *Proceedings of the Fifteenth Colloid Symposium*, Cambridge, 1938.
- [15] J. Eggers, M. A. Fontelos, C. Josserand, and S. Zaleski, "Drop dynamics after impact on a solid wall: Theory and simulations," *Physics of Fluids* 22, 062101, 2010; doi: 10.1063/1.3432498.
- [16] N. Laan, K. G. de Bruin, D. Bartolo, C. Josserand, and D. Bonn, "Maximum Diameter of Impacting Liquid Droplets," *Physical Rev Applied* 2, 044018, 2014.
- [17] C. J. Forster, "Parallel Wavelet-Adaptive Direct Numerical Simulations of Multi-Phase Flows With Phase Change, Ph.D. Thesis, Georgia Institute of Technology, August 2016.
- [18] T. Bodnár, A. Sequeira, and M. Prosi, "On the shear-thinning and viscoelastic effects of blood flow under various flow rates," *Applied Mathematics and Computation* 217, 2011.
- [19] S. Mandre and M. P. Brenner, "The mechanism of a splash on a dry solid surface," *J. Fluid Mech.* 690 (2012) 148-172.
- [20] L. Xu, W. W. Zhang, and S. R. Nagel, "Drop splashing on a dry smooth surface, *Phys. Rev. Lett.* 94 (2005), pp. 184505:1-4.

## VI. Dissemination of Research Findings

1. Lockard, M., Neitzel, G. P., & Smith, M. K., "Droplet Impact Patterns on Inclined Surfaces with Variable Properties," Sixty-Seventh Meeting of the American Physical Society - Division of Fluid Dynamics, San Francisco, CA, November 23–25, 2014.
2. Lockard, M., "The Fluid Dynamics of Droplet Impacts on Inclined Surfaces with Application to Forensic Blood spatter Analysis," M.S. Thesis, Georgia Institute of Technology, August 2015.
3. Smith, M. K., Lockard, M., & Neitzel, G. P., "Droplet Impact on Inclined Surfaces for Forensic Bloodstain Analysis," Sixty-Eighth Meeting of the American Physical Society - Division of Fluid Dynamics, Boston, MA, November 22–24, 2015.
4. Forster, C. J., "Parallel Wavelet-Adaptive Direct Numerical Simulations of Multi-Phase Flows With Phase Change, Ph.D. Thesis, Georgia Institute of Technology, August 2016.
5. Forster, C. J. and Smith, M. K. "GPU-based Wavelet-adaptive Multiphase Flow Simulation for All Mach Numbers. Part 1: Verification of High-speed Compressible Flow," submitted to J. Comp. Physics, 2016.
6. Forster, C. J. and Smith, M. K. "GPU-based Wavelet-adaptive Multiphase Flow Simulation for All Mach Numbers. Part 2: Verification of Low-speed Compressible Flow," in preparation for submission to J. Comp. Physics, 2017.